ELSEVIER

Journal of Nuclear Materials 251 (1997) 34–48

journal of nuclear materials

Computer simulation of vacancy and interstitial clusters in bcc and fcc metals

Yu.N. Osetsky [a,1], M. Victoria [b], A. Serra [a,*], S.I. Golubov [c], V. Priego [a]

[a] *Universitat Politecnica de Catalunya, Gran Capitan s / n, E-08034 Barcelona, Spain*
[b] *Ecole Polytechnique de Lausanne, CRPP-Fusion Technology, CH-5232 Villigen PSI, Switzerland*
[c] *Institute of Physics and Power Engineering, Bondarenko sq.1, 249020 Obninsk, Russia*

Abstract

Interstitial clusters in bcc-Fe and fcc-Cu and vacancy clusters in fcc-Cu have been studied by computer simulation using different types of interatomic potentials such as a short-ranged empirical pair potential of Johnson type, short-ranged many-body potentials of Finnis–Sinclair type and long-ranged pair potentials obtained within the generalized pseudopotential theory. The stability of a self interstitial in bcc-Fe was found to be dependent on the range of potential but not on the type. Thus, both short-ranged potentials simulated ⟨110⟩ dumb-bell as a stable configuration while in the case of the long-ranged potential the stable configuration is the ⟨111⟩ crowdion. Nevertheless the structure and properties of interstitial clusters were found to be qualitatively the same with all the potentials. Up to 50 interstitials, the most stable clusters were found as perfect dislocation loops with Burgers vector $\vec{b} = \frac{1}{2}\langle 111\rangle$. The stability of interstitial clusters in Cu also does not depend on the potential and for the same sizes the most stable configurations are faulted Frank loops $\frac{1}{3}\langle 111\rangle\{111\}$ and edge loops in the {110} plane. The structure and stability of vacancy clusters in fcc-Cu were found to be dependent mainly on both the range of potential and equilibrium conditions. Thus for long-ranged non-equilibrium pair potentials vacancy clusters in the {111} plane collapsed and formed vacancy loops or stacking fault tetrahedra depending on the shape of the initial vacancy platelet. For the short-ranged equilibrium many-body potential vacancy clusters do not collapse into loops or tetrahedra. The process of vacancy clustering in the cascade region has been studied by molecular dynamics. This study has been done for the case of a PKA energy of about 20–25 keV. We found that the processes simulated with the short-ranged many-body potential and the long-ranged pair potential are qualitatively different. Thus for the many-body potential we have observed melting and crystallization of the central part of the cascade region, sweeping of vacancies inside due to the moving of the liquid–solid interface and increasing of vacancy concentration in the centre of the cascade region; however no significant clustering was observed. Contrarily for the long-ranged pair potential we have observed a very fast diffusion in the solid crystallite and the formation of stacking fault tetrahedra. The results obtained have been discussed and compared with the experimental data. © 1997 Elsevier Science B.V.

1. Introduction

Interstitial and vacancy clusters are important components of the microstructure observed when metals are irradiated with energetical particles. Therefore the knowledge of the properties, formation and growth mechanisms of these clusters is essential for understanding and predicting the effects of radiation damage. Extensive computer simulation studies of cascade phenomena carried out during the last decade have estimated some qualitative processes having taken place. The success was achieved in the study of interstitial clustering and mobility of small interstitial clusters formed in the cascade region [1–3]. These results are in accordance with the modern model of point defects cascade production bias [4]. As far as vacancy clustering is concerned the results obtained are not so significant. It was found that the main mechanism of the increasing of vacancy concentration in the centre of the

* Corresponding author. Tel.: +34-3 401 6886; fax: +34-3 401 6504; e-mail: serra@etse.ccpb.upi.es.

[1] On leave from Radiation Materials Science Department, Russian Research Centre 'Kurchatov Institute'.

0022-3115/97/$17.00
PII S0022-3115(97)00255-9

cascade region on the stage of thermal spike is the sweeping of vacancies due to the movement of the liquid–solid interface during the crystallization of the previously melted zone. As a result of this process the vacancy concentration grows up to several percent. Nevertheless none of computer simulation has observed significant vacancy clusters. There can be two reasons for this, small statistics of the high energy cascade simulations and/or the interatomic potentials used for those simulations.

Due to the big CPU resources needed for cascade simulations mainly short-ranged many-body potentials have been used. Many-body potentials constructed within different models such as embedded atom, second order tight binding and Finnis–Sinclair empirical model have been successfully used in many other than cascade studies, for example dislocations and grain boundaries, surfaces, thermodynamical properties and defects in alloys, interstitial clusters, etc. Unfortunately there are very few studies of vacancy clusters and vacancy clustering processes made with these potentials. We want to underline here that we did not find in the literature any successful study of defects like vacancy loops (VL) and stacking fault tetrahedra (SFT). At the same time long-ranged pair potentials developed within different models of the pseudopotential theory have been successfully applied to the study of vacancy clusters and vacancy clustering processes in bcc, fcc and hcp materials [5–10]. The results obtained are in qualitative agreement with the experimental results on the formation vacancy loops and stacking fault tetrahedra under irradiation.

In this paper we present some results of a comparative study of vacancy and interstitial clusters carried out with potentials of different types. The aim of this study was to find the common and different features of the results obtained with potentials of different types and to try to understand what characteristics of the potentials may influence in the study of defect clusters production and properties.

2. Interatomic potentials and calculation model

We have used different types of interatomic potentials such as short-ranged pair (SRPP), long-ranged pair (LRPP) and many-body potentials (MBP). To SRPP we relate potentials which include interactions up to the second nearest neighbours. They are mainly empirical potentials constructed 15–20 years ago. To long-ranged we relate potentials which include interactions with third neighbours and further. They are potentials obtained within the second order pseudopotential model. We should underline that all many-body potentials used are short-ranged potentials.

For the study of interstitials in the bcc-Fe we have chosen the well known Johnson potential [11] which is SRPP, a Finnis–Sinclair type potential constructed in Ref. [12] which is MBP and the potential constructed within a pair approximation of the generalised pseudopotential theory [13] which is LRPP. All the potentials were fitted to the elastic constants and vacancy formation energy. MBP and LRPP reproduce well the P–V diagrams, anharmonic properties, phonon dispersion, etc. The main difference in the properties calculated with the potentials is the different stability of self interstitial atoms. Thus, Johnson potential reproduces the ⟨110⟩ dumb-bell as the most stable configuration (the difference in energy formation of ⟨111⟩ crowdion and ⟨110⟩ dumb-bell is $\Delta E = 0.28$ eV), MBP reproduces a smaller difference in energy $\Delta E = 0.07$ eV, while LRPP gives ⟨111⟩ crowdion as the most stable configuration with $\Delta E = -0.14$ eV. Provided the stability of interstitials may be important for the interstitial clusters properties, we studied the origin of this difference. We found that the range of the potential is the main feature responsible for the stability of a self interstitial atom either in ⟨110⟩ dumbbell or in ⟨111⟩ crowdion configuration. As a general trend we found that the longer the range the more stable is the ⟨111⟩ crowdion. Thus, for LRPP a decrease in the cut off radius leads to an increase in the stability of ⟨110⟩ dumb-bell. When this potential is restricted to its first well the ⟨110⟩ dumb-bell was found to be 0.18 eV more stable than the ⟨111⟩ crowdion. The opposite effect has been found for Johnson potential. It is possible to make ⟨111⟩ crowdion more stable than ⟨110⟩ dumb-bell by increasing the cut off radius just for $0.12a$ (that means before the next co-ordination sphere) without any change in static properties. We did not study the MBP; however we have found in literature that the same effect was observed with an EAM potential for bcc-Fe [14]. The potentials for bcc-Fe are plotted in Fig. 1 where the many-body potential is in the effective pair form.

For the study of interstitials and vacancies in the fcc-Cu we have used MBP constructed in Ref. [15] and the LRPP potential described in Ref. [13]. The potentials have been fitted to elastic constants and vacancy formation energies. Some properties reproduced with the potentials are presented in Table 1. A comparison of these data demon-

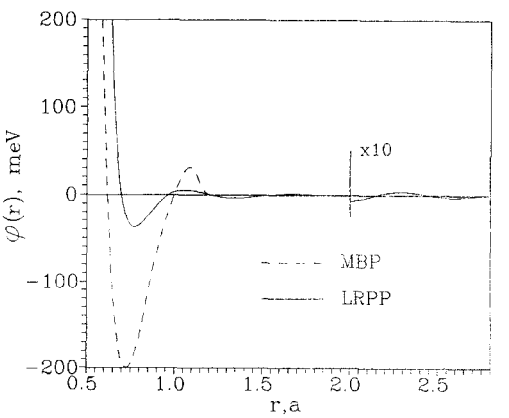

Fig. 1. Effective interatomic potentials for bcc-Fe.

strates that the majority of properties are very close. The formation energy of vacancy and interstitial atom obtained with LRPP are slightly higher than for MBP and both potentials reproduce ⟨100⟩ dumb-bell as the most stable self interstitial configuration. We did not find any effect of the potential range to the relative stability of SIA in fcc-Cu. Both potentials reproduce well the phonon spectra, P–V diagrams and the fcc structure as the most stable. The MBP and LRPP potentials for Cu are presented in Fig. 2. Besides, to compare our results with some previous studies we have used the empirical potential constructed in Ref. [16] (CU1) and the potential constructed in Ref. [5] within the pseudopotential theory (CU2). According to the above criterion CU1 and CU2 potentials are long-ranged potentials.

The results described here have been obtained with static and molecular dynamics simulations. It follows a short description of the main features of the calculation models. For the static simulation we have used spherical crystallites with the usual fixed boundary conditions. To relax the crystallite we applied a combination of conjugate gradients static relaxation and the quasidynamical method. Such a combination leads the system close to the global minimum of the potential energy. For the biggest defects studied the maximum effective local temperature was estimated as ≈ 350–450 K (see Ref. [17]). For the molecular dynamic simulation we used cubic crystallites with periodical boundary conditions (for interstitial diffusion) and spherical crystallites with fixed boundary conditions (thermal spike and evolution of the depleted zone). To integrate the equation of motion we applied the Verlet algorithm

Table 1
Comparison of the properties calculated with long-ranged pair potential (LRPP) and short-ranged many-body potential (MBP) for Cu. Elastic constants B, C, C_{44} in Gpa, monovacancy and ⟨100⟩ dumb-bell self interstitial energies (E_V^f, E_I^f) and volume (V_V^f, V_I^f) formation, vacancy migration energy E_V^m, divacancy binding energy (E_{2V-1}^b, first neighbours, E_{2V-2}^{bf}, second neighbours) (all energies in eV, volumes in equilibrium atomic volume), intrinsic stacking fault energy γ_I in mJ/m^2, linear coefficient of thermal expansion α_I in 10^{-6} K^{-1}

	LRPP	MBP	Experiment
B	139	137	139
C	24	24	24
C_{44}	83	75	76
E_V^f	1.49	1.19	1.2–1.4
E_V^m	0.78	–	0.71
V_V^f	0.78	0.77	0.75–0.85
E_{2V-1}^b	0.07	0.17	–
E_{2V-2}^{bf}	0.01	−0.03	–
E_I^f	3.72	3.62	2.2±0.7
V_I^f	0.30	–	0.55±0.2
α_I	17.8	–	16.7
γ_I	35	36	30–50

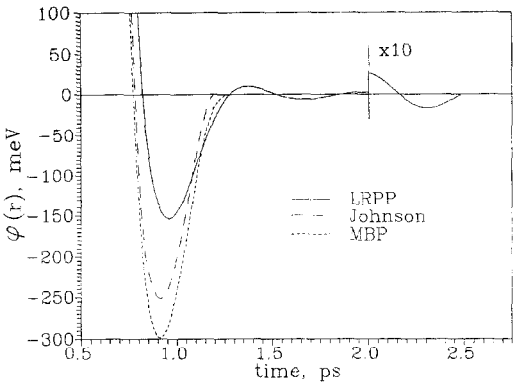

Fig. 2. Effective interatomic potentials for fcc-Cu.

with a variable time step. The criterion for the determination of time step has been discussed in Ref. [18].

Special attention has been paid to the analysis of the vacancy clusters configuration. For monitoring the vacancy migration during diffusion before clustering we have used ATOMTV code, however the visualization of vacancies is not an appropriate method to study vacancy clusters after they collapse into VL or SFT. The configuration of atoms have been studied using the projection of atoms to different cross-sections. To imitate a three dimensional character of two-dimensional cross-sections we defined the size of every symbol to be proportional to the distance between the corresponding atom and cross-section plane. The minimum size was related to the distance $-0.5d_p$ (d_p is interplanar distance for the corresponding plane) while the maximum to the distance $+0.5d_p$. Such a method is very good when the configuration that has to be analyzed contains the group of atoms displaced similarly from the perfect positions.

3. Results

3.1. Interstitials in bcc-Fe and fcc-Cu

3.1.1. Self interstitial diffusion in Fe

The diffusion of self interstitial atoms has been studied using LRPP and Johnson short-ranged pair potentials by molecular dynamics in a cubic crystallite of 4394 mobile atoms with the usual periodical boundary conditions (for a more detailed description see Ref. [18]). During the simulation mean square displacements and jump frequencies were calculated. We have also analyzed every jump from the point of view of the mechanism and type of the defect jumped. For each temperature about 1500–2000 jumps were counted. It was found that the interstitial migration mechanism depends on the temperature for both potentials. Thus for the lowest temperature (300–400 K) mainly jumps via the ⟨111⟩ crowdion mechanism were observed while for the highest temperature studied (1800–1900 K)

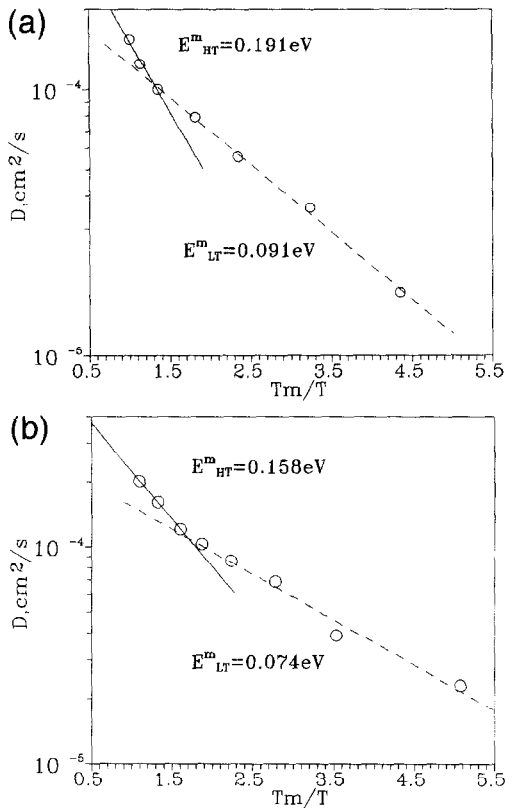

Fig. 3. Self interstitial diffusion coefficient versus reciprocal temperature: (a) Johnson potential, (b) LRPP.

the major part of jumps were ⟨110⟩ dumb-bell in the ⟨111⟩ direction. For the intermediate temperatures we have observed jumps of both types and the contribution of each type depends on the temperature. This combination of two mechanisms has been reflected in the temperature behaviour of the diffusion coefficients calculated using mean square displacements (see Fig. 3a and b). For simplicity in Fig. 3 we indicated only two different regions with their migration energies. However we should note that the linear behaviour of the diffusion coefficient appears only for high and low temperatures where only one mechanism takes place. For the intermediate temperatures there are contributions of the two mechanisms and therefore the slope is temperature dependent. The high temperature results presented in Fig. 3a are in good agreement with the results reported earlier in Ref. [19] for high temperature and a very similar potential.

The same qualitative results have been obtained in Ref. [20] for the above described MBP for bcc-Fe.

3.1.2. Interstitial clusters in Fe and Cu

We simulated planar clusters containing up to 50 interstitials with initial habit planes {100}, {110} and {111}. The modelled system was a spherical crystallite with a rigid boundary. The number of mobile atoms N_α was varied from ≈ 1800 to ≈ 19000. In this study we have used three potentials for bcc-Fe and two potentials for fcc-Cu. To study the thermal stability of clusters we heated a previously relaxed configuration and aged it during time t_{aging} monitoring the configuration and calculating the mean square displacements. Aging time has been varied from a few tens to a few hundreds ps depending on the temperature. A more detailed description of the structure and properties of interstitial clusters in Fe and Cu will be presented elsewhere. Here we give only qualitative information about stable clusters in Fe and Cu simulated with different potentials.

First of all we want to underline that, in general, qualitative stability of the interstitial clusters does not depend on the potentials used for each particular metal. This means that although the values of formation and binding energy are different for different potentials nevertheless all the potentials describe the same types of stable clusters.

Thus, in bcc-Fe the most stable clusters are found to be perfect dislocation loops with Burgers vector $\frac{1}{2}\langle 111\rangle$. These loops can be either in {110} or in {111} planes. Clusters simulated in other planes tend to rotate into {111} planes. This rotation depends on the plane and size of the cluster. For example clusters in {100} plane were found to be unstable and during the above described procedure of relaxation they rotated completely. The degree of rotation for clusters initially created in {110} plane depends on the number of interstitials. Small clusters ($N_I \leq 3$–5, N_I, number of interstitials) have almost the same stability in {110} or {111} planes. In both cases they were a set of ⟨111⟩-crowdions collected in the corresponding planes. Clusters of about 5–15 interstitials were rotated partially into a plane somewhere in between {110} and {111} while the clusters containing more than 19 SIA were rotated completely. According to the criteria discussed in Ref. [21] these clusters are equivalent to pure edge loops with the Burgers vector $\vec{b} = \frac{1}{2}\langle 111\rangle$. They can be interpreted as well as a set of ⟨111⟩-crowdions in the {111} plane. By limiting the movement of atoms during the relaxation one can stabilize small clusters (< 14 SIA) in the {110} plane. These clusters are metastable and after heating the crystallite they rotate into a {111} plane completely.

It should be noted that in Refs. [21,22] the small interstitial clusters (up to 16 atoms) have been studied with the same SRP and with a MBP similar to the one used here. They reported that clusters initially created in {110} plane were rotated to {111} plane which was the same process that has been observed in the present work.

Another stable configuration for an interstitial cluster in Fe is a set of ⟨100⟩ crowdions. These clusters can be in either {110} or {100} planes and can be described as perfect or edge dislocation loops with the Burgers vector $\vec{b} = \langle 100\rangle$. The stability of such clusters depends on size and shape. The most stable clusters are rhombic in {110}

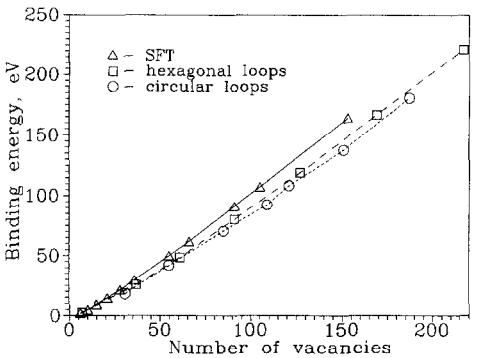

Fig. 4. Binding energy versus number of vacancies in the different clusters relaxed with the LRPP.

(or square in {100}) plane when they are simulated with the long-ranged pair potential. These clusters are dynamically stable and the binding energy of rhombic clusters of 16 and more interstitials is very much close to the binding energy of $\frac{1}{2}\langle 111\rangle$ perfect loops.

In fcc-Cu two types of stable interstitial clusters were found, faulted and perfect dislocation loops. Small clusters up to about 4–5 SIA can be stable in all the planes as a set of $\langle 100\rangle$ dumb-bells or $\langle 110\rangle$-crowdions. Clusters of bigger sizes are most stable in the plane {110} where they form a configuration equivalent to the pure edge dislocation loop with Burgers vector $\vec{b} = \frac{1}{2}\langle 110\rangle$. Clusters in {100} plane are unstable and they rotate into {110}. The stability of clusters in {111} plane depends on their shape. Thus, clusters of a hexagonal and circular shape are very stable and they form Frank loops with Burgers vector $\vec{b} = \frac{1}{3}\langle 111\rangle$. The binding energy of Frank loops is slightly lower than those for perfect loops. The dynamical stability of faulted loops again depends on their shape. Thus, hexagonal and circular clusters are very much stable while rhombic and irregular clusters are not thermally stable and transform into perfect $\frac{1}{2}\langle 110\rangle$ loops. For example the initially relaxed rhombic faulted loop $\frac{1}{3}\langle 111\rangle\{111\}$ of 16 SIA heated up to 850 K transformed into $\{110\}1/2\langle 110\rangle$ after about 6 ps while hexagonal faulted cluster of 7 SIA was stable at all studied temperatures (up to 1000 K).

Again, as in the case of bcc-Fe, perfect loops can be interpreted as sets of crowdions collected in the plane perpendicular to the close-packed direction (which is the direction of crowdion).

Only the absolute value of the energetical properties were potential dependent.

Therefore in both Fe and Cu we have found two types of stable interstitial clusters. In Fe these are perfect dislocation loops with Burgers vectors $\frac{1}{2}\langle 111\rangle$ and $\langle 100\rangle$. Both loops are glissile. In Cu stable clusters can be sessile Frank loops or glissile perfect loops with Burgers vector $\frac{1}{2}\langle 110\rangle$. In general, these results are consistent with the experimentally observed types of dislocation loops in irradiated Fe and Cu.

3.2. Vacancy clusters in fcc-Cu

We have studied vacancy clusters in the {111} plane. Initially vacancy platelets of hexagonal, circular (polygons with more than six sides) and triangular shapes were created in the central plane. Then the crystallite was relaxed and the final configuration was analyzed.

3.2.1. Long-ranged pair potential

The results of the calculated binding energy for all the clusters studied are presented in Fig. 4. The most significant relaxation was found for the initially triangular platelets. For these clusters we have observed an asymmetric relaxation and the formation of stacking fault tetrahedra (SFT). Although for small clusters the final configuration is dependent on the size, for clusters of $N_V \geq 28$ (N_V is the number of vacancies) the final configuration is a well defined SFT. As an example we present in Fig. 5 {111}

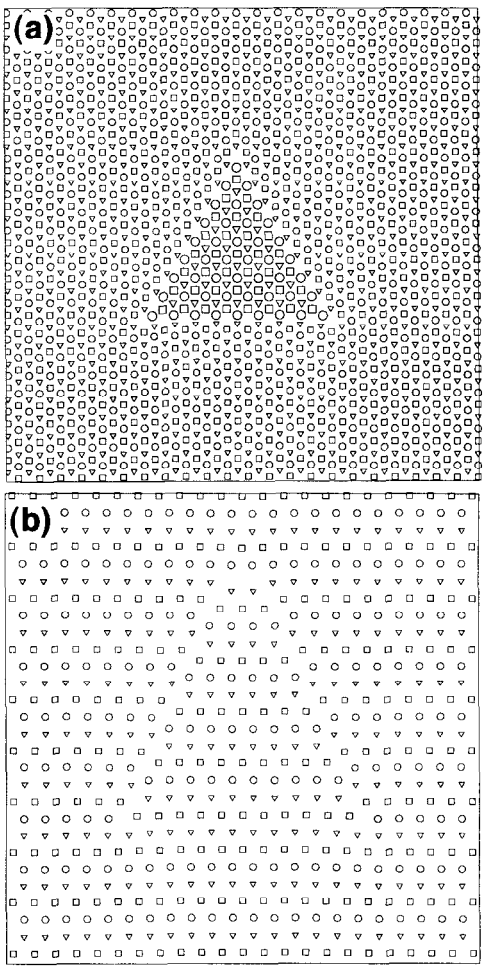

Fig. 5. Cross-sections through the centre of a crystallite containing a SFT of 136 vacancies relaxed with the LRPP. (a) {111}, (b) {112}.

and {112} cross-sections through the centre of a SFT obtained after the relaxation of a triangular platelet of $N_V = 136$. It is easy to recognize that the {111} cross-section gives the better image of the SFT.

For the hexagonal platelet it was found that the final configuration depends on the size. Thus, for a small loop with $N_V = 7$ we have observed an almost symmetric relaxation. However, for bigger loops the relaxed configuration was rather complicated. In general we found that a big enough loop tends to transform into six tetrahedra, three of them located above the habit plane and three others below. The length of tetrahedra sides is close to the length of the initial hexagon side oriented along the ⟨110⟩ direction. The feature of such a configuration can be found for clusters with $N_V \geq 19$. As an example in Fig. 6 we present three sets of {111} cross-sections of the configuration obtained after the relaxation of a cluster with $N_V = 217$. Fig. 6a is the projection of atoms in the original platelet plane (squares) together with the nearest planes above (triangles) and below (circles). The sizes of the symbols indicate the position of the corresponding atom perpendicular to the cross-section plane. Fig. 6b and c are similar projections in the next three planes above (b) and below (c) the central planes. Fig. 6a shows that the tetrahedra are truncated in the centre of the hexagonal platelet where the atoms from the upper and lower planes form a stacking fault. The relative ratio of this stacking fault depends on the size of the loop and it increases for bigger loops. Other cross-sections of the three upper and three lower tetrahedra and their truncated character can be seen in Fig. 6b and c.

For small circular platelets we found that almost a symmetric relaxation resulted in a faulted vacancy loop with a Burgers vector $\vec{b} = \frac{1}{3}\langle 111\rangle$. In case of a circular platelet with $N_V \geq 31$–35 we found a configuration similar to those after the relaxation of the hexagonal platelet. That means we have observed a trend to dissociate into tetrahedra near the edges of circular platelets elongated along ⟨110⟩ directions. In general, these tetrahedra were truncated more than for the hexagonal platelet of the same size. With an increasing size of circular loops the ratio of the central stacking fault increases and the degree of dissociation decreases. An example of a big circular loop ($N_V = 421$) can be seen in Fig. 7.

We have also studied the thermal stability of small vacancy clusters. We found that small circular loops transform into SFT at a high enough temperature. For example a circular loop of 31 vacancies heated at 950 K after 55 ps has transformed into a SFT of 28 vacancies. The other three vacancies were accumulated outside on the face of the SFT. The transformation was very fast, lasting about

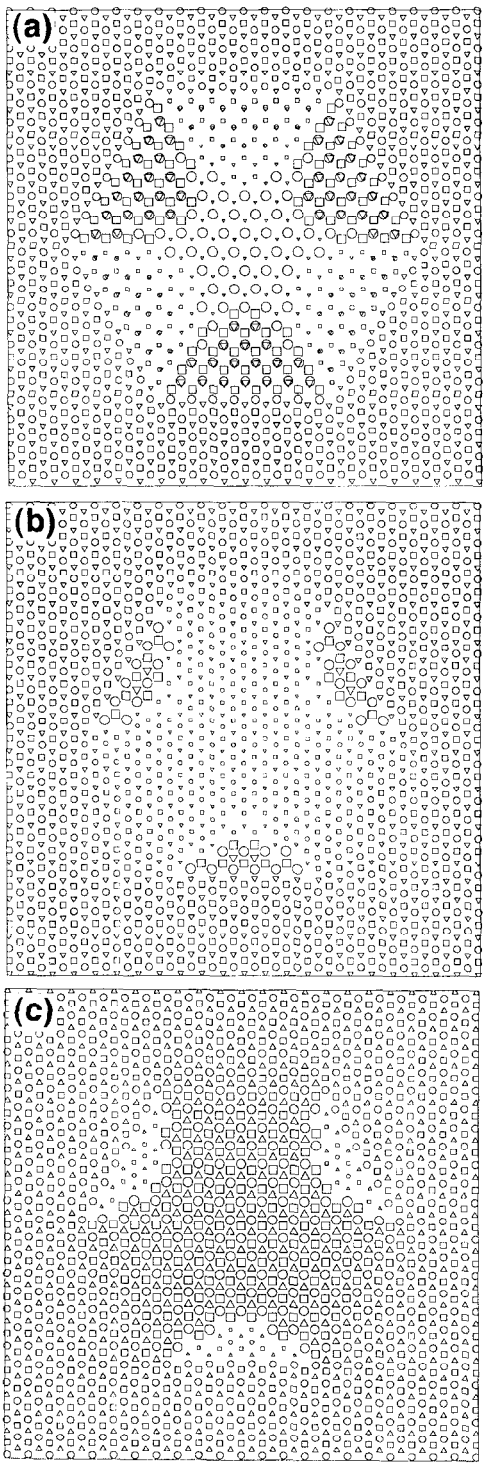

Fig. 6. (111) cross-section of the hexagonal vacancy loop of 217 vacancies relaxed with the LRPP: (a) The planes plotted are the habit plane labelled as $N_p = 0$ (○), and planes above $N_p = 1$ (△) and below $N_p = -1$ (□); (b) $N_p = 2$ (□), 3 (○), 4 (△). Note that the biggest symbols correspond to atoms displaced from the planes above ($3 \rightarrow 2$, $4 \rightarrow 3$ and $5 \rightarrow 4$) (c) $N_p = -4$ (□), -3 (○), -2 (△). Note that the smallest symbols correspond to atoms displaced from the planes below ($-3 \rightarrow -2$, $-4 \rightarrow -3$ and $-5 \rightarrow -4$).

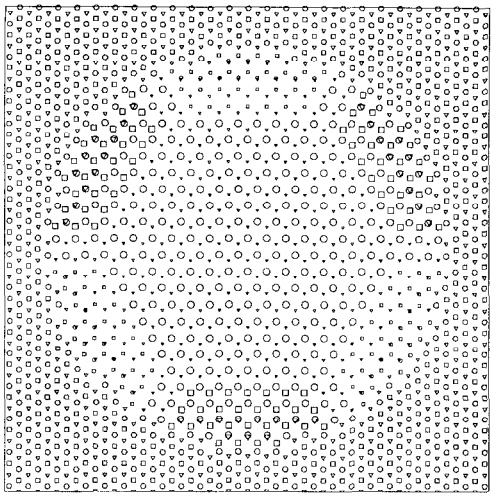

Fig. 7. (111) cross-section through the habit plane of the circular loop of 431 vacancies relaxed with the LRPP.

3–5 ps, and we found that is not a diffusional transformation. A more detailed description will be presented elsewhere.

3.2.2. Short-ranged many-body potential

Qualitatively different results were obtained using the MBP. We have found very small relaxation energy and displacements after the relaxation for all the clusters studied. For example, for a hexagonal loop with $N_V = 91$ the relaxation energy for MBP was $E_{91}^r = 0.93$ eV while for LRPP $E_{91}^r = 82.26$ eV. The typical relaxed configuration is presented in Fig. 8 as a {112} cross-section through the centre of a triangle cluster with $N_V = 136$, the same as presented in Fig. 5b for LRPP. The difference in structures obtained with different potentials can be clearly seen. Note

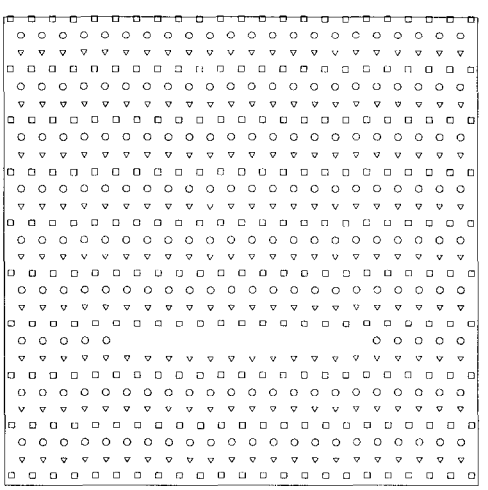

Fig. 8. {112} cross-section through the centre of a triangular cluster of 136 vacancies relaxed with the MBP.

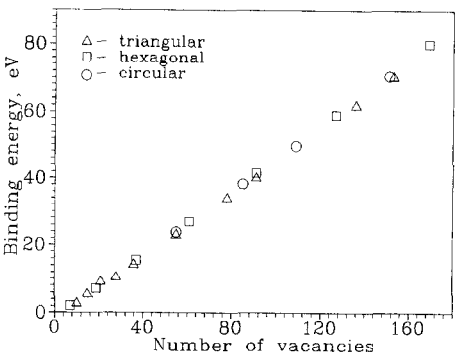

Fig. 9. Binding energy versus number of vacancies in the different clusters relaxed with the MBP.

that there is no difference in the relaxation of circular, hexagonal and triangular clusters with MBP and this is reflected in Fig. 9 where the binding energies for all the clusters follow the same dependence.

Thus, relaxation of the same defects results in different configurations for the above potentials. The LRPP potential undergoes much bigger relaxation and collapse of vacancy platelets. Provided the MBP is very short ranged and equilibrium, all the displacements near defects are strongly localized. So we decided to check whether the configurations obtained after the relaxation with the MBP are the most stable or if there is a barrier which prevents the relaxation from a more stable configuration. To do this the collapsed configurations obtained with the LRPP have been used as initial configurations for further relaxation with the MBP. After the post-relaxation we have analyzed the configurations and calculated the difference in binding energy of these new configurations and the configurations obtained after relaxing only with MBP (ΔE). It was found that configurations obtained after post-relaxation are exactly the same as after relaxation with the LRPP with a small difference in absolute value of displacements. However, the difference in binding energy ΔE depends on the size and type of clusters. This can be seen in Fig. 10 where

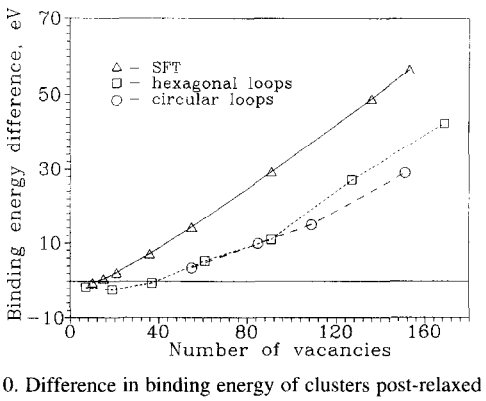

Fig. 10. Difference in binding energy of clusters post-relaxed with the MBP from the initially collapsed configurations and clusters relaxed only with the MBP.

ΔE for different clusters is plotted versus N_V. Thus, for big enough clusters ΔE is positive and it grows with the size of clusters.

For small clusters we found that, although the post-relaxation keep the starting collapsed structure, the binding energy decreases in comparison with the configurations obtained only with the MBP. This can be seen in Fig. 10 for clusters containing less than 12–40 vacancies depending on the configuration. This result is rather surprising because for such small clusters the displacements are not big. For example the maximum displacement for a hexagonal loop of 19 vacancies relaxed with the LRPP is about $0.05a$. Nevertheless the MBP did not return the system to its more stable configuration. These results again confirm that the MBP has some barriers between very close configurations.

We want to note here that the other pair potentials mentioned above as CU1 and CU2 demonstrated the same results as the LRPP, namely collapse into VL and SFT and dissociation of loops into tetrahedra.

Therefore, we can conclude that for the simulation of vacancy clusters the choice of potential can affect the results. Thus the long-ranged pair potential used here allows results to be obtained which are consistent with the experimental data in general, Frank loops and stacking fault tetrahedra are the most stable vacancy clusters. However the short-ranged many-body potential does not reproduce such results in simple static simulations although it can describe a high stability of Frank loops and SFT created somehow (for example relaxed with the LRPP).

3.3. Vacancy clusters formation under thermal spike conditions

To check the effect of the potential on the process of clustering of vacancies inside a cascade region during the thermal spike cooling we have simulated the following model.

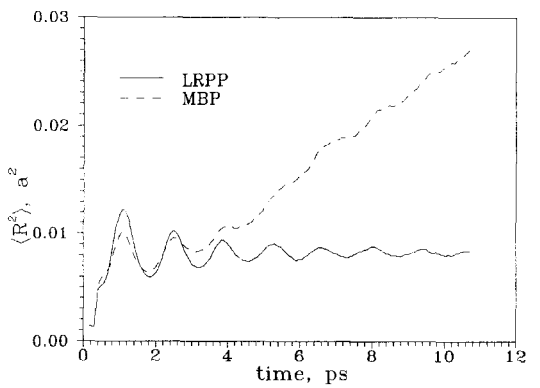

Fig. 11. Mean square displacements during the equilibrating process.

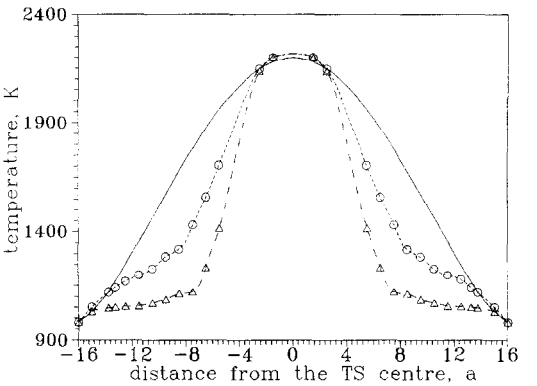

Fig. 12. Steady state temperature distribution in the perfect crystallite. ————, theory; ○, LRPP; △, MBP.

First of all we prepared a crystallite with a stationary thermal spike. To do this we generated a thermal spike corresponding to the chosen primary knock-on atom energy (E_{PKA}) inside a spherical crystallite. The stationary thermal gradient was then obtained after a relatively long time simulation when the central part of the crystallite was heated and the outer region was cooled together with the damping of the displacement waves generated by the thermal spike. For a crystallite of radius $16a$ (a, lattice parameter of Cu) containing ≈ 70000 mobile atoms and a thermal spike equivalent to $E_{PKA} \approx 22$ keV it took about 12 ps to establish a steady state.

Starting from this stage we have found different behaviour for the potentials. Thus, the MBP model had a central region melted after about 4.5 ps. Contrary to that, the LRPP model kept the crystalline structure. This can be seen in the temporal evolution of the mean square displacements for both potentials (Fig. 11).

The steady state temperature distribution for both potentials is presented in Fig. 12. There are some differences in the temperature profiles, for example, the profile obtained for LRPP in general can be related to a bigger value of the lattice thermal conductivity.

In the second stage, we introduced a chosen vacancy distribution inside the equilibrated crystallite. Then the heating was stopped and the crystallite was cooled down from the boundary layer according to a chosen rate of cooling. Here we only present some results obtained after cooling of a thermal spike corresponding to $E_{PKA} \approx 22$ keVwith a vacancy rich region of spherical shape (radius $5a$, mean vacancy concentration $C_V = 5$ at.%, vacancies are distributed randomly) simulated with the many-body and long-ranged pair potentials for Cu described above.

We have simulated three events for every potential. Although this statistic is rather poor, it allowed us to find some qualitative differences in the process simulated with different potentials. The typical evolution of the temperature in the centre of the crystallite is presented in Fig. 13. One can see that the time to cool the crystallite with LRPP

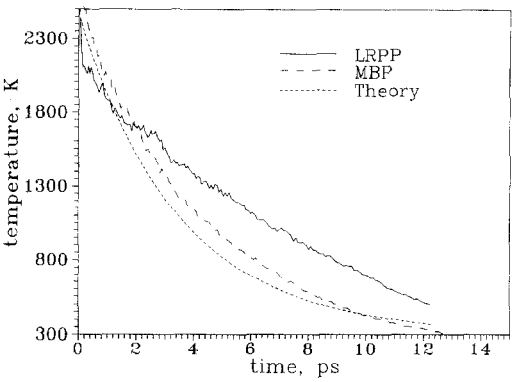

Fig. 13. Temperature in the central region versus time of thermal spike cooling.

is bigger than for MBP. This is rather surprising because, as we noted above, the stationary temperature distribution in the perfect crystallite demonstrates that the thermal conductivity simulated with the LRPP is higher. In Section 3.3.1 we will give a possible explanation for this effect.

3.3.1. Short-ranged many-body potential

The melted region started to crystallize at about 2 ps after the starting of cooling. During the crystallization process we have observed the increasing of the vacancy concentration due to the sweeping of vacancies by the solid–liquid interface moving towards the centre of the crystallite. In general this process, melting, crystallization and sweeping vacancies to the centre of melted region, has been observed and studied earlier in full cascade simulations [23,24]. As a result of this process about 70–80% of vacancies were concentrated near the centre of the crystallite and other vacancies were distributed around mainly as mono- and di-vacancies.

To identify the configuration of bigger vacancy clusters we analysed sequential cross-sections in the different planes. A cluster, for example SFT, could be identified if several cross-sections present the features observed in the equivalent cross-section obtained after a static simulation of the corresponding defect as was described in Section 3.2. In two simulations we could not clarify the configuration of the vacancy rich regions after the thermal spike was cooled. These regions consist of a few hundred atoms separated by an irregular system of stacking faults. The inner structure was found to be fcc with a number of stacking faults, vacancies and small vacancy clusters. It is interesting to note that in many cases the shape of stacking faults was triangular. However these stacking faults did not form any regular system which could be interpreted as a tetrahedron. Only in the third simulation, together with such a kind of region, we could observe some configuration which can be described as a strongly truncated stacking fault tetrahedron.

The detailed study of the evolution of this region shown that during cooling it was split into two regions of different sizes. The smaller region resulted in a half truncated SFT while the other one did not transform into a regular vacancy cluster. As an example, we present cross-sections of the crystallite with the above two objects in Fig. 14. One can see clearly the cross-section of the truncated SFT (can be compared with Fig. 5a) and the other vacancy rich region. The size of the biggest stacking fault was equivalent to the SFT formed from 28–36 vacancies. However, the specific sequence of atoms was observed only for four–five adjacent {111} planes (instead of 7–8 planes for the perfect SFT). It is difficult to estimate the real number of vacancies concentrated in such a cluster and probably instead of truncated tetrahedron we should refer to the formation of some specific configuration of stacking faults.

3.3.2. Long-ranged pair potential

For the LRPP we did not observe melting neither during the equilibrating process nor after introducing the vacancy population though there was a significant disordering in the central region after inserting vacancies. We have observed two processes. The first one was disordering during the first 1.0–1.5 ps. Later, when the temperature fell to about 1800 K, the process of ordering started. This process was accompanied by energy release. It can be seen in Fig. 13 that this energy is bigger than the latent heat of melting for the MBP. This can be one of the reasons of increase of the total time for cooling. Further evolution included the process of solid state diffusion and increasing of the vacancy concentration in the central region. The process of clustering started when the temperature in the crystallite centre decreased to about 1350 K (this was about 3 ps after cooling started). This process is going together with the further ordering and both of them

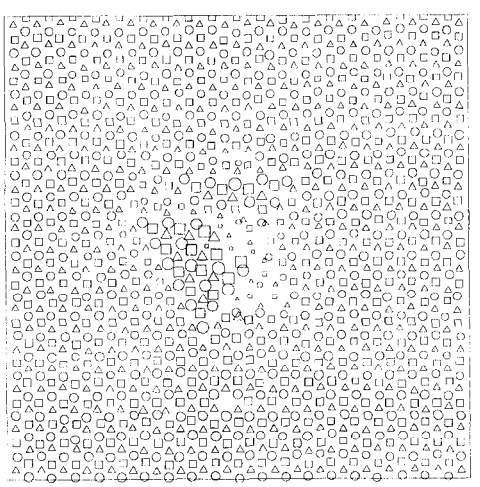

Fig. 14. Cross-section of the crystallite cooled with the MBP.

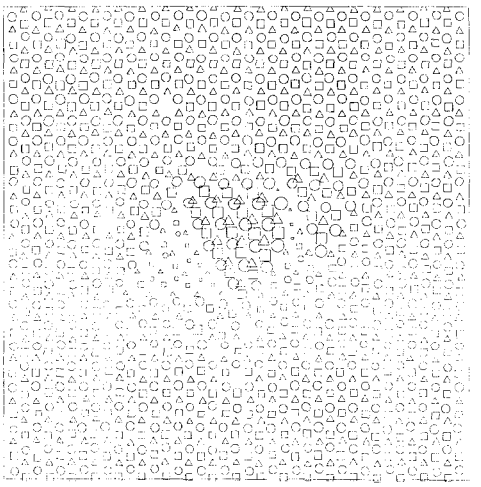

Fig. 15. Cross-section of the crystallite cooled with the LRPP.

are accompanied by the energy release which is due to the binding and ordering energy. During this stage we have observed nucleation and growth of the SFT close to the centre of the crystallite. Note that the total increase in vacancy concentration obtained for LRPP is smaller than for MBP. However, in the case of the LRPP vacancy clusters always have been formed. In all three simulations we found that about 30–60% of vacancies are clustered into one or two clusters. It was difficult to estimate the precise number of vacancies in the clusters because all the tetrahedra were not perfect. So we considered the size of the biggest face and estimated the number of vacancies as for the perfect SFT of the equivalent size. In total we observed one SFT of 28 vacancies, a SFT of the same size together with a small SFT of 10 vacancies and two neighbouring SFT of 21 vacancies differently oriented. The last case can be interpreted as a rhombohedral vacancy loop dissociated into two tetrahedra. The {111} cross-section of this configuration is presented in Fig. 15. One can see two areas of triangular shape filled up with symbols of bigger and smaller sizes, these are the bases of two differently oriented tetrahedra. Similar dissociation of a rhombohedral vacancy platelet has been observed in static simulations.

4. Discussion

4.1. Interstitials in bcc-Fe and fcc-Cu

In general the results obtained for small interstitial clusters in Fe and Cu have common features. In both lattices the clusters up to about 40–50 interstitials are most stable as pure edge dislocation loops in the plane perpendicular to the close-packed direction. In both cases the clusters are formed by a set of crowdions and therefore we assume that they are glissile. This is in good agreement with the suppositions of the point defects cascade production bias model [4] and allows one to understand the mobility of small interstitial clusters observed in molecular dynamics simulation of cascades in bcc and fcc metals [1,2,25,26]. The difference in results is in the high stability of Frank loops in Cu. Therefore, in Cu sessile interstitial Frank loops can be formed apart of glissile perfect loops. This is in qualitative agreement with the experimental results.

The results obtained here shown that the dynamical behaviour of mono-interstitials in bcc-Fe and the relative stability of the clusters in Fe and Cu does not depend on the potentials used.

Thus in the case of Fe we used potentials that reproduce different stability for mono-interstitials, nevertheless, the temperature behaviour of the interstitial migration mechanisms was qualitatively the same. Moreover all the stable configurations can be performed as a set of ⟨111⟩-crowdions. That means the stable configuration obtained by static simulation at zero temperature does not determine the dynamical behaviour and structure of small clusters. As it was demonstrated above, the difference in the stable configuration of self interstitial is dependent on the range of the potentials but not on the type. So it is difficult to make any conclusion about the applicability of one or another potential to the interstitial study. On the one hand there is experimental evidence that the stable self interstitial configuration is ⟨110⟩ dumb-bell. So one has the possibility of using a short-ranged potential which would reproduce this stability keeping in mind that this configuration is not stable under low temperature and it may change to the dynamical crowdion. However, such kind of potentials cannot describe a low temperature dumb-bell diffusion. Experiments show rather big interstitial migration energy of about 0.3 eV [27] which cannot be attributed to crowdion unless another interpretation of the experimental results is found. On the other hand the idea of one-dimensional glide of small interstitial clusters is accepted and there are some evidences in computer simulation [1,2,25,26]. To our point of view all the potentials used here are able to reproduce this effect provided they present the interstitial cluster as a set of ⟨111⟩ crowdions. We should note that there is at least one short-ranged EAM potential which reproduces a statically and dynamically stable ⟨110⟩ for a wide temperature region and one-dimensional glide of di- and tri-interstitials [26]. We do not know the details of this simulation and potential but we assume it should be very short ranged. In the case of Cu both potentials reproduce the most stable mono-interstitial configuration as a ⟨100⟩-dumbbell while the stable configuration of small clusters is a set of ⟨110⟩-crowdions.

A surprising result is that, in both cases, the most stable configurations for small interstitial clusters are the set of crowdions (oriented along close packed directions) concentrated into a plane perpendicular to the close packed direction. This is in contradiction with the accepted mecha-

nism when point defects concentrate into close packed planes as clusters with stacking fault and during further growth they may unfault when the energy of stacking fault is big enough. We should note that this mechanism works well for vacancy loops in Fe [28,29] and for the initial stage of growth of vacancy loops in Cu [5,6,17]. However, the results obtained here for Fe and Cu and the results obtained in Refs. [21,22] for Fe show that this mechanism may not work in case of interstitial clusters. To understand this, a careful study of big enough interstitial loops have to be done. The simulation of loops of size of ≈ 2–4 nm (200–300 interstitials) will allow to compare the structure and Burgers vector with the experimental data. This work is in progress now.

4.2. Vacancy clusters in fcc-Cu

The situation with vacancy clusters is somehow more clear than with interstitials. It is known from experiments that vacancy loops and stacking fault tetrahedra can be formed under cascade irradiation, during aging of quenched metals and under deformation. So the potentials that are used for the study of vacancy clusters formation and evolution should be able to reproduce these defects. At the moment there are at least two models describing how vacancy clusters can be formed. The first one based on vacancy clustering into {111} platelet with the following collapse into VL or SFT depending on the shape. The second one is the direct formation of the SFT in the cascade region due to a process similar to phase transformation in the vacancy rich regions. The last model has been confirmed at the simulation of the evolution of cascade depleted zones in Cu using different pair potentials [7–10,30].

The results discussed here show that the short-ranged many-body potential of Finnis–Sinclair type do not reproduce the collapse of vacancy platelets into VL or SFT in a static simulation. It is necessary to apply an additional influence to collapse clusters. Moreover, small collapsed clusters are not stable with the MBP used here and the binding energy of the uncollapsed clusters is rather low. That means the efficiency of their nucleation and growth is small and it may be difficult to nucleate and grow them via adding vacancies one by one as it is supposed in quenching experiments. But if a big enough VL or SFT could be created it would be stable under such a MBP.

The short range and equilibrium character of the MBP can be the reason of its behaviour in the relaxation of vacancy platelets. On one hand the same behaviour was described by Johnson [31] who simulated vacancy clusters in Ni using a short-ranged equilibrium pair potential, and on the other hand, other long-ranged and non-equilibrium potentials used here (CU1, CU2) and in Refs. [5,6,16] simulate the relaxation into VL or SFT. Another consequence of the short range and equilibrium character of potentials to the vacancy–vacancy interaction and vacancy mobility in the cascade depleted zone will be discussed in Section 4.3.

Using the LRPP we have studied the mechanisms of growth and shrinkage of the SFT [17]. We have found that small tetrahedra can grow effectively up to a size of about 100 vacancies but there are some mechanisms (related to the dislocation jog movement) which make growth difficult for SFT of bigger sizes. This result is in agreement with the experimental observation of SFT in Cu (formed under irradiation and deformation) where the size distribution has its maximum at about 2.4 nm (70–80 vacancies) [32]. Besides, this can give an additional explanation as to why big vacancy loops observed in experiments do not dissociate so clearly into six tetrahedra. The dissociation of loops should stop when the size of the possible tetrahedra is beyond the critical size for tetrahedra growth. These arguments can be additional proof that for such a kind of properties the non-equilibrium and long range character of the potential can be important.

4.3. Melting of fcc-Cu under different conditions

Provided the melting process and temperature are widely used when thermal spike model is used, lets expose some considerations about experimental melting in relation to MD simulation.

First of all the thermodynamic melting temperature (T_m) estimated through the calculation of the free energy for solid and liquid phases [33] is not coincident with the much higher temperature (T_{MD}) for which a perfect crystal becomes unstable under an MD simulation. Although the lattice defects such as grain boundaries and free surface decrease the T_{MD} [34] it is clear that a simulation cannot include all the stochastic effects and the final result is still higher than T_m. Besides the problem of simulation of a 'real' crystal, there is a problem of simulation of the 'real' physical time needed for an equilibrium melting. Therefore the maximum time allowed for simulation will influence the value of the lower temperature able to melt or, at least, highly disorder the crystal [35]. The thermal spike evolution occurs during very short time, within a very small region and under high pressure therefore it is a question whether the region is melted or just disordered.

Data for melting were obtained for the MBP in Ref. [36]. It was estimated that the equilibrium melting temperature was about 1200–1300 K. This is in agreement with our results using the same potential provided we have observed that during the equilibrating process the existence of a liquid–solid interface was related to the temperature 1250–1300 K. Taking into account the high internal pressure in the system we may estimate 1200–1250 K as the highest limit for the equilibrium melting temperature. This temperature is about 100–150 K lower than the experimental one (1356 K).

To obtain a melting temperature for the LRPP we used a special simulation using the Parinello–Rahman constant

pressure technique [37] for a crystallite of 1384 mobile atoms. We found that the time necessary to melt with LRPP is much higher than for MBP. For instance we have observed melting at 1900 K after 27 ps, at 1700 K after 59 ps and at $T = 1550$ K after 359 ps. To simulate possible effects of the lattice defects we included a vacancy concentration of 0.4 at.% (five vacancies randomly distributed in the crystallite of 1384 atoms). At about 1500 K we observed melting after 57 ps. Based on these results we have estimated the upper limit for melting temperature for LRPP as 1500–1550 K. Note that in Ref. [37] for a similar long-ranged potential for Cu the melting temperature was estimated as 1400 K.

Thus the difference in melting temperature obtained with MB and LRPP is rather big and it correlates with the difference in vacancy formation energy (see Table 1). However, more important is the difference in the kinetics of the melting process observed for these potentials; to melt a system with LRPP potential one should apply either very high level of overheating or long enough time. Moreover it can happen that even a large overheating is not enough to start melting within a small volume at high pressure. As we mentioned above, the central region of the crystallite with the LRPP at the end of the equilibration process was strongly disordered and when a depleted zone was created the level of disorder increased. During this process (about 1 ps) the central region stored a significant potential energy which can be seen in the temperature evolution curve (Fig. 13). However for real melting the time was too small. We carried out a special treatment to be sure that the observed disordering was not a melting. The main difference between a disordered state and liquid is the self-diffusion coefficient which is supposed to be much higher in liquid. We have calculated the dependence of mean square displacements (MSD) in the whole crystallite versus time and versus temperature in the central region. One variant of this dependence versus time is presented in Fig. 16 for both potentials. One can see that in the case of MBP the main part of MSD have been created within the first 5 ps that is during the evolution of the melted region. In the case of LRPP there is one peak in MSD which can be related to the maximum disordered state of the central region. There are no features which can be related to the diffusion in liquid state.

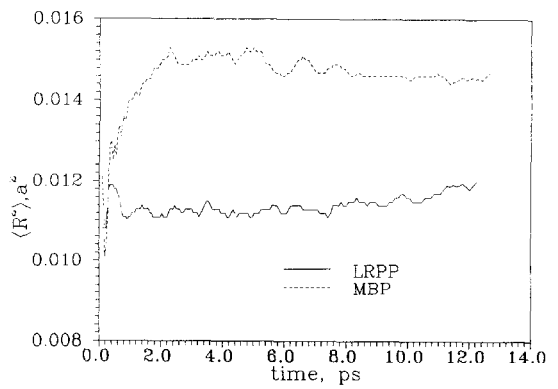

Fig. 16. Temporal evolution of the mean square displacements during thermal spike cooling.

4.4. Diffusion of vacancies at thermal spike conditions in Cu

The result presented in Fig. 16 shows that for the MBP all mean square displacements were created mainly in the melted state. After crystallization ($t = 5$ ps) one can observe a decrease in the MSD. This is proof of a very slow diffusion in the solid state. On the contrary, in the case of LRPP there is a continuous increase in MSD that means an active diffusion process.

This difference in diffusional behaviour for different potentials has been tested with an additional study. We have simulated the evolution of the same vacancy rich region under constant temperatures in the range 700–1150 K during 250 ps. For the LRPP the increase of vacancy mobility appears at 700–850 K. At 950 K the fast diffusion leads to clustering after about 120–150 ps. About 50–60% of vacancies were clustered and the diffusion process has been slowed down. For 1150 K we observed an increase of vacancy concentration (but not a real clustering) and fast diffusion in this region. In the case of the MBP we did not observe any increase in mobility for 700–900 K. More or less significant diffusion was found at temperatures of 950–1100 K. The system has been split into several local regions where we could see diffusion of small vacancy clusters like di- and tri-vacancies without any trend to form big clusters. Of course 250 ps is too short a time to study a general diffusion but it is enough for cascade applications. This study is not finished yet, however, we can give some preliminary conclusions. First, with the MBP the vacancy–vacancy interactions are weak and do not lead to a significant increase in vacancy mobility. We did not observe any significant clustering as a result of diffusion. Second, with the LRPP the vacancy–vacancy interactions are stronger and lead to the increase in vacancy mobility. The increase in mobility depends on the vacancy concentration until the clustering starts. The active clustering starts at a temperature of $\approx$ 900–1000 K.

4.5. Formation of vacancy clusters in fcc-Cu under thermal spike conditions

Taking into account the above additional information about vacancy mobility inside a vacancy rich region let us try to discuss the possible mechanisms of clusters formation that have been simulated here.

The situation with LRPP is rather clear. The effect of increasing vacancy mobility has been found for bcc-Fe [38] in a simulation with long-ranged pair potential. This

effect in fcc-Cu has been confirmed in the present work but with an additional contribution, there is the general difference in the stability of vacancy clusters in bcc and fcc structures. The binding energy of a small cluster is much higher in fcc metals (especially in Cu) than in bcc ones. That is why in the previous study of the vacancy mobility in bcc-Fe [38] this effect was found even for very high vacancy concentration up to 15 at.%. For Cu we found that the increase of vacancy mobility versus vacancy concentration has a saturation related to the formation of clusters. Just the SFT has been formed those vacancies do not contribute more to the diffusion because of the very high stability of tetrahedron. So for the LRPP there is an increase of vacancy mobility in the vacancy rich region followed by a strong clustering. In addition, concerning the specific conditions of thermal spike, there is an additional mechanism for sweeping vacancies inside the hot region due to the anisotropic vacancy diffusion in the temperature gradient [39]. These mechanisms allow the system to create big enough clusters for the short time of the thermal spike evolution. This cluster or, rather region with a very high vacancy concentration transforms into a SFT during the thermal spike cooling. During this transformation we did not observe any vacancy clustering into a triangular cluster in {111} plane. Stacking fault tetrahedra formed directly in the vacancy rich regions through the formation of four ordered stacking faults. In this respect SFT is not a vacancy cluster formed through a vacancy by vacancy growth, as is expected under aging conditions. At cascade conditions it is just an energetically favourable way to redistribute vacancies over stacking faults in the region with a very high vacancy concentration.

In case of the MBP the main mechanism is the sweeping of vacancies due to the movement of the liquid–solid interface of the previously melted region. As shown in special studies [40,41] this effect is very strong and it may create a very big local vacancy concentration. But then, after the crystallization, the evolution of this vacancy rich region (with a vacancy concentration up to 15–20 at.%) continues in the crystalline state. However, for the MBP there is not a significant effect of the vacancy concentration to the diffusion and the binding energy of small clusters is not big enough to perform an effective clustering. Though, under thermal spike conditions, there exists the possibility of cluster collapse when there are big fluctuations in the local pressure and stress. Therefore it is possible that MBP reproduces the formation of SFT. In Section 3.2.2 it is stabilized that under MBP the SFT are stable if local conditions like high pressure and stress allow the collapse by overpassing the energetical barrier. Comparing both potentials it can be established that the main difference between results with LRPP and MBP is the probability of SFT formation. For LRPP it is about 100% because the formation of SFT does not demand any barrier. For the MBP the probability depends on the barrier and on the local conditions in the vacancy rich region.

There is another interesting question to discuss related to the different time of cooling obtained for the two potentials. The steady state temperature distribution established at the end of the equilibrating process (Fig. 14) shows that in general the lattice thermal conductivity simulated with the LRPP is higher than for the MBP. However, the crystallite with the MBP has been cooled faster. We found two possible reasons why the cooling in the case of the LRPP was delayed. First, the energy stored in the disordered region during the equilibration process and the initial time of cooling (up to about 1 ps) for the LRPP is much bigger than the latent melting heat for the MBP. In that case during the ordering process this energy can be released as an additional heating of this region. Second, some additional heating can be related to the clustering process. For example the binding energy for SFT of 28 vacancies is 21.6 eV. This energy is enough to heat 1000 atoms more than 150°C. Provided that there are other small clusters and that the process of clustering is going during few ps it can end in a significant delay of cooling time.

5. Summary and conclusions

The properties of interstitial and vacancy clusters and the cascade depleted zone evolution during thermal spike cooling have been studied using potentials of different types. The results received allow to find some features which can be related to the potentials and others which are not dependent on the potentials used.

The main results obtained are as follows.

(1) The interstitial diffusion mechanism in bcc-Fe depends on the temperature and changes from crowdion to dumb-bell when the temperature increases. Qualitatively this result is independent on the interstitial stable configuration at 0 K.

(2) Up to 50 SIA, the stable clusters in both fcc-Cu and bcc-Fe are sets of crowdions oriented along a close packed direction and concentrated in one plane perpendicular to this direction. They can also be described as edge dislocation loops in the {111} and {110} planes for Fe and Cu, respectively. Another stable configuration of interstitial clusters in Cu is a faulted Frank loop $\frac{1}{3}\langle 111\rangle\{111\}$.

(3) Vacancy clusters in fcc-Cu are stable in the {111} plane from where they may collapse into stacking fault tetrahedra or faulted vacancy loops depending on the shape.

(4) Small vacancy loops can be then dissociated into one or several SFT depending on the particular configuration of the loop. The most regular dissociation was observed for hexagonal loops which dissociate into six truncated tetrahedra of the same size. The degree of dissociation decrease when the size of the loop increase. Loops with diameter bigger than 3 nm are $\frac{1}{3}\langle 111\rangle\{111\}$ Frank loops.

(5) The result obtained in this and previous studies show that small ($N_I \leq 50$) interstitial clusters are stable in planes perpendicular to closed packed directions whereas vacancy clusters are more stable in closed packed planes.

The properties that are potential dependent are as follows.

(1) The stability of self interstitials in bcc-Fe depends on the cut-off radius. The stable configuration goes from ⟨110⟩-dumb-bell to ⟨111⟩-crowdion with the increase of the range irrespectively of the type of potential.

(2) The relaxation process found for vacancy clusters in Cu depends on the range of the potential and its equilibrium character.

(3) The melting process in fcc-Cu is much faster if it is simulated with a short-ranged equilibrium potential in comparison with the LRPP which needs a bigger overheating too.

(4) The diffusion in the high vacancy concentration region has a much significant increase for nonequilibrium long-ranged potentials than for equilibrium short-ranged both in fcc-Cu and in bcc-Fe [38]. We attribute this difference to the influence of the internal pressure and range of potential in the vacancy–vacancy interaction.

(5) The process of thermal spike cooling simulated by MBP describes melting and sweeping of vacancies by the movement of the solid–liquid interface. No intensive clustering of vacancies is observed. If the simulation is done with a LRPP, there is no melting and the diffusion in the vacancy rich region is strongly accelerated. Intensive clustering leads to the creation of SFT.

It is difficult to make an explicit conclusion about what potential is better. One of the aims of the paper was to find the common and different qualitative results for different potentials. As we have found the main difference is in the results of vacancy clusters simulation and in the processes taking place during the thermal spike evolution (melting, diffusion inside vacancy rich region, mechanisms of clustering). For example, it is well known that in fcc metals, particularly in Cu, aging after quenching leads to the formation and growth of vacancy type dislocation loops and/or stacking fault tetrahedra. The results obtained here show that this type of event can be more easily described with the long-ranged pair potentials (LRPP, CU1, CU2). The thermal spike evolution in Cu is much more difficult to analyze because many different physical processes take place there at the same time. In principle, for both potentials, it is possible to get vacancy clusters although in case of the LRPP the probability is much higher. However, the way *how* vacancy clusters have been formed is qualitatively different. Therefore, it is important to understand which scenario of thermal spike evolution is more realistic. To clarify which potential gives a more realistic approach, there are some physical processes that should be studied in detail. Among them we want to mention melting under thermal spike conditions. We believe that a special computer simulation study of this process together with the analysis of experiments on a very fast heating and cooling in metals could help to solve the problem.

And finally we want to underline that according to our and previous studies the difference in results is not due to the different character of the interactions described by potentials (many-body or pair) but mainly due to the difference in the range of interactions and in the equilibrium properties of potentials.

Acknowledgements

We are grateful to Professor D. Bacon and Dr B. Singh for numerous discussions of the experimental and simulation results. This work was supported by the project INTAS-93-3454-EXT, grants from Swiss National Research Fund and CIRIT (Y.O.) and the project PB93-0971-C03 of Spanish DGICYT.

References

[1] T. Diaz de la Rubia, M. Guinan, Phys. Rev. Lett. 66 (1991) 2766.
[2] A.J.E. Foreman, W.J. Phythian, C. English, Philos. Mag. A66 (1992) 671.
[3] D.J. Bacon, T. Diaz de la Rubia, J. Nucl. Mater. 216 (1994) 275.
[4] B. Singh, A.J.E. Foreman, Philos. Mag. A66 (1992) 975.
[5] N.Q. Lam, L. Dagens, N.V. Doan, J. Phys. F13 (1983) 2503.
[6] M.J. Sabochick, S. Yip, N.Q. Lam, J. Phys. F18 (1988) 349.
[7] V.G. Kapinos, Yu.N. Osetsky, P.A. Platonov, J. Nucl. Mater. 165 (1988) 286.
[8] V.G. Kapinos, Yu.N. Osetsky, P.A. Platonov, J. Nucl. Mater. 170 (1990) 66.
[9] V.G. Kapinos, Yu.N. Osetsky, P.A. Platonov, J. Nucl. Mater. 173 (1990) 229.
[10] V.G. Kapinos, Yu.N. Osetsky, P.A. Platonov, J. Nucl. Mater. 184 (1991) 127.
[11] R.A. Johnson, Phys. Rev. 134 (1964) 1329.
[12] G.J. Ackland, D.J. Bacon, A. Calder, T. Harry, Philos. Mag. A75 (1997) 713.
[13] Yu.N. Osetsky, A.G. Mikhin, A. Serra, Philos. Mag. A56 (1995) 361.
[14] G. Simonelli, R. Pasianot, E.J. Savino, Mater. Res. Soc. Symp. Proc. 291 (1993) 567.
[15] G.J. Ackland, G. Tichy, V. Vitek, M.V. Finnis, Philos. Mag. A56 (1987) 735.
[16] A. Englert, H. Tompa, R. Bullough, in: Fundamental Aspects of Dislocation Theory, Nat. Bureau of Standards, Special Publication No. 317 (NBS, Washington, 1970) p. 273.
[17] Yu.N. Osetsky, M. Victoria, A. Serra, S.I. Golubov, Philos. Mag. (1997) to be published.
[18] Yu.N. Osetsky, A. Serra, Def. Diffus. Forum 143–147 (1997) 155.
[19] D.H. Tsai, R. Ballough, R.C. Perrin, J. Phys. C3 (1970) 2022.
[20] D.J. Bacon, T. Harry, unpublished.
[21] R. Bullough, Perrin, Proc. Roy. Soc. A305 (1968) 541.

[22] D.J. Bacon, J.M. Harder, J. Nucl. Mater. 155–157 (1988) 1254.
[23] T. Diaz de la Rubia, R.S. Averback, R. Benedek, W.E. King, Phys. Rev. Lett. 59 (1987) 1930.
[24] T. Diaz de la Rubia, R.S. Avarback, H. Hsieh, R. Benedek, J. Mater. Res. 4 (1989) 579.
[25] R. Stoller, G.R. Odette, B.D. Wirth, these Proceedings, p. 49.
[26] N. Soneda, T. Diaz de la Rubia, unpublished report.
[27] F.W. Young Jr., J. Nucl. Mater. 69&70 (1978) 441.
[28] V.G. Kapinos, Yu.N. Osetsky, P.A. Platonov, Phys. Status Solidi (b)155 (1989) 373.
[29] V.G. Kapinos, Yu.N. Osetsky, P.A. Platonov, J. Nucl. Mater. 173 (1990) 229.
[30] C.C. Matthai, D.J. Bacon, J. Nucl. Mater. 135 (1985) 173.
[31] R.A. Johnson, Philos. Mag. 16 (1967) 533.
[32] Y. Dai, M. Victoria, to be published (1997).
[33] S.M. Foiles, J.B. Adams, Phys. Rev. B40 (1989) 5909.
[34] S.R. Phillot, S. Yip, D. Wolf, Comput. Phys. 6 (1989) 20.
[35] Yu.N. Osetsky, A. Serra, Phys. Rev. B (1996) to be published.
[36] V.G. Kapinos, D.J. Bacon, Phys. Rev. B50 (1994) 13194.
[37] M. Parinello, A. Rahman, J. Appl. Phys. 52 (1981) 7182.
[38] V.G. Kapinos, Yu.N. Osetsky, P.A. Platonov, J. Nucl. Mater. 184 (1991) 211.
[39] V.G. Kapinos, P.A. Platonov, Radiat. Eff. 103 (1987) 45.
[40] V.G. Kapinos, D.J. Bacon, Philos. Mag. A68 (1993) 1165.
[41] H. Van Swygenhoven, A. Caro, Phys. Rev. Lett. 70 (1993) 2098.